Effect of the Activation Force of Mechanophore on Its Activation Selectivity and Efficiency in Polymer Networks

Zhi Jian Wang[1,#], Shu Wang[2,#], Julong Jiang[3], Yixin Hu[2], Tasuku Nakajima[1,4], Satoshi Maeda[1,3], Stephen L. Craig[2,*], Jian Ping Gong[1,4,*]

[1]Institute for Chemical Reaction Design and Discovery (WPI-ICReDD), Hokkaido University, Sapporo 001-0021, Japan.

[2]Department of Chemistry, Duke University, Durham, NC 27708-0346, USA.

[3]Department of Chemistry, Faculty of Science, Hokkaido University, Sapporo 060-8628, Japan.

[4]Faculty of Advanced Life Science, Hokkaido University, Sapporo 001-0021, Japan.

ABSTRACT: Over the recent decades, more than 100 different mechanophores with a broad range of activation forces have been developed. For various applications of mechanophores in polymer materials, it is crucial to selectively activate the mechanophores with high efficiency, avoiding non-specific bond scission of the material. In this study, we embedded cyclobutane-based mechanophore crosslinkers (I and II) with varied activation force (f_a) in the first network of the double network hydrogels and quantitively investigated the activation selectivity and efficiency of these mechanophores. Our findings revealed that crosslinker I, with a lower activation force relative to the bonds in the polymer main chain (f_a-I / f_a-chain = 0.8 nN / 3.4 nN), achieved efficient activation with 100% selectivity. Conversely, an increase of the activation force of mechanophore II (f_a-II / f_a-chain = 2.5 nN / 3.4 nN) led to a significant decrease of its activation efficiency, accompanied by a substantial number of non-specific bond scission events. Furthermore, with the coexistence of two crosslinkers, significantly different activation forces resulted in the almost complete suppression of the higher-force one (i.e., I and III, f_a-I / f_a-III = 0.8 nN / 3.4 nN), while similar activation forces led to simultaneous activations with moderate efficiencies (i.e., I and IV, f_a-I / f_a-IV= 0.8 nN / 1.6 nN). These findings provide insights into the prevention of non-specific bond rupture during mechanophore activation and enhance our understanding of the damage mechanism within polymer networks when using mechanophores as detectors. Besides, it establishes a principle for combining different mechanophores to design multiple mechanoresponsive functional materials.

1. Introduction

Recent years have seen the rapid development of polymer mechanochemistry, which endows polymer materials with various functions,[1-3] including self-reporting of stress/strain/damage through color change,[4-10] mechanical property enhancement,[11-16] and force-responsive small molecule release.[17-19] These functions are usually based on mechanoresponsive units, known as mechanophores, that translate external mechanical force to chemical signals. Currently more than 100 different mechanophores with a broad range of force-coupled reactivity and functionality have been developed, for example, azoalkane,[20,21] spiropyran,[4,8,22] cyclobutane,[13,16,23-25] etc. When incorporating these mechanophores into a polymer network, the activation efficiency of mechanophores is often a key concern. Activation efficiency refers to the fraction of embedded mechanophores that are successfully activated under external forces. It is a crucial factor as it directly influences the strength of the resulting chemical signal and subsequent mechanoresponsive functions in polymer materials. To enhance activation efficiency, strategies such as lowering the activation force of mechanophores[26,27] and optimizing the surrounding network structure have been proven to be effective.[8,28,29]

In addition to activation efficiency, the separate but related concept of activation selectivity is equally important but has received relatively less attention. When the load is exerted on the mechanophore, the load is also distributed in the connected polymer backbone, which can potentially lead to unintended bond breakages. These bond breakages lower the activation efficiency of the mechanophore and generate unexpected chemical signals (usually mechanoradicals) that might interfere with the desired mechanochemical response. Moreover, ambiguity surrounding the sites of scission may lead to a misunderstanding of the fracture mechanism when using mechanophores as detectors.[30] For example, a recent study gives qualitative evidence of non-specific bond scission when PEG chains with less reactive mechanophores are exposed to ultrasound in a solution state,[27] and similar effects have been observed in a study of acrylates with a chain-centered coumarin mechanophore.[31] Quantitative characterization of the selectivity of mechanophore activation is still lacking, however, most notably in bulk polymer materials.

In addition to the issues mentioned above, most research in mechanochemistry have focused on the use of a single mechanophore in the material to achieve a single mechanoresponsive function. With the rapidly growing

toolkit of available mechanophores and their associated diverse range of function, combinations of mechanophores are increasingly realistic targets for multiply mechanoresponsive materials.[6] Reports of such materials remain very limited, however, in part because the simultaneous activation of distinct mechanophores with different force-coupled reactivity remains challenging. We were therefore motivated to investigate the efficiency and selectivity of mechanophore activation within a common material system as a function of combination of multiple mechanophores with differing reactivity.

In this work, we incorporated cyclobutane mechanophores with varying activation forces as crosslinkers of the first network of double network (DN) hydrogels and quantitatively investigated how the activation force of cyclobutane mechanophores affects its activation selectivity and efficiency under mechanical force. We first elucidated the competition between the activation of a single cyclobutane mechanophore motif and the non-specific scission of other bonds in the polymer network (**Figure 1a**). We then extended the study to the competition between two mechanophores that are incorporated into the same network (**Figure 1b**).

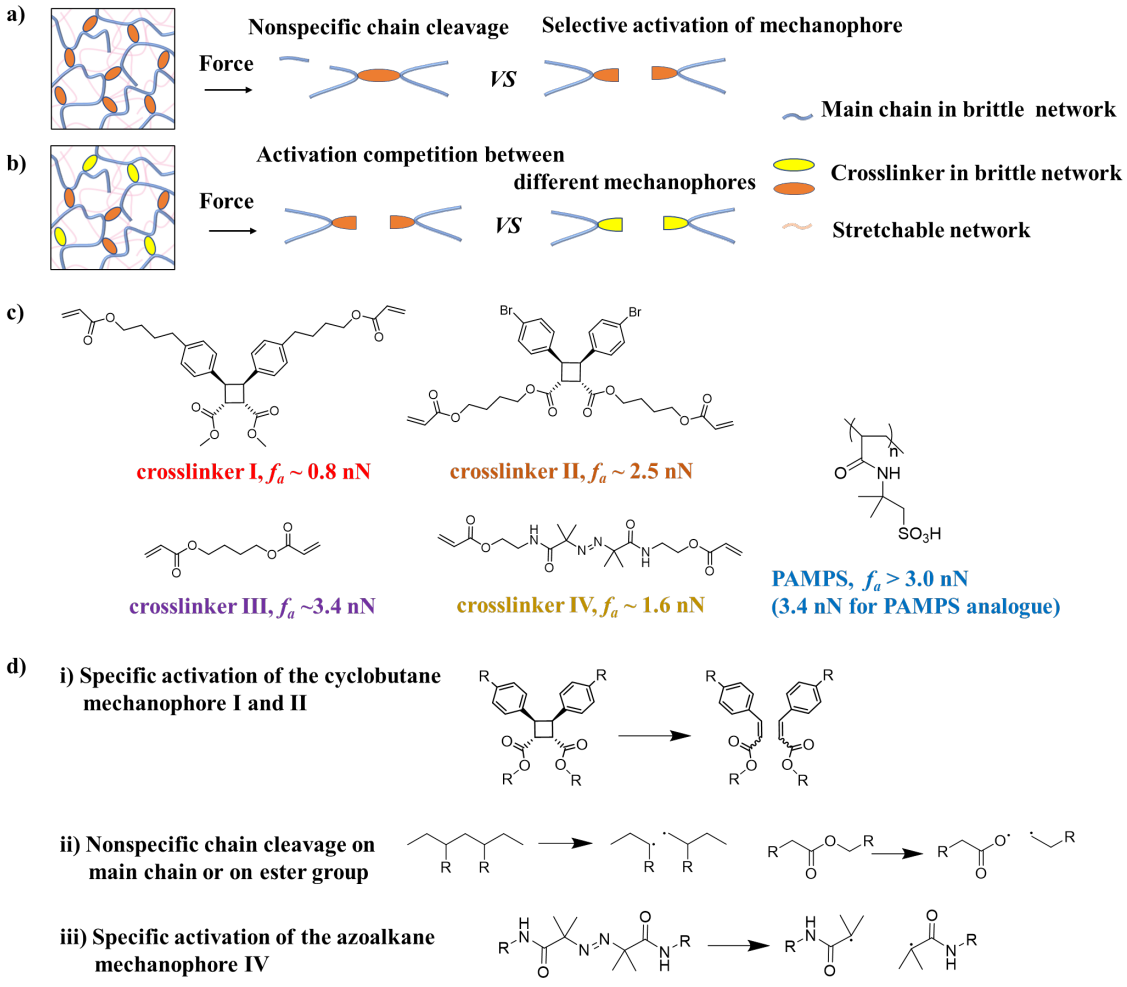

Figure 1. Schematic illustration of the cyclobutane-based mechanophore activation in competition with nonspecific bond rupture and other mechanophore activation. In this work, mechanophores are used as crosslinkers incorporated into the first brittle network of double network hydrogels. (a) Illustration of the competition between the selective activation of mechanophore in the crosslinker and nonspecific bond rupture in the main chain backbone. (b) Illustration of the activation competition between different mechanophores. (c) Chemical structure of the crosslinkers and the main chain adopted in this work and their corresponding activation force. (d) Force-induced activation of cyclobutane mechanophore generates C=C bonds and forms the cinnamate group (i) while non-specific bond rupture on mainchain backbone or on ester group (ii) or activation of azoalkane group (iii) generates mechanoradicals.

2. Design principle

We chose to study the activation of cyclobutane-based mechanophores that are embedded in the first network of DN hydrogels, which are an excellent material platform to study polymer mechanochemistry.[32] We adopted DN gels consisting of two interpenetrating polymer networks with contrasting mechanical properties. The first network is a highly crosslinked brittle poly(2-acrylamido-2-methyl-1-propanesulfonic acid) (PAMPS), and the second network is a loosely crosslinked stretchable polyacrylamide (PAAm).[33] In a double network with components of such contrasting

properties, the applied mechanical stress is predominantly carried by the first network, which efficiently activates the bond rupture in the first network, whereas the interpenetrating second network absorbs stress of the first network released by the bond rupture.[34,35] Via this mechanism, the stress concentration is mitigated within the surviving first network, and probability of bond activation is controlled by the external force. Accordingly, this DN structure allows for a much higher number of bond rupture events compared with a conventional single network,[12] which increases the total number of mechanically triggered chemical events and their accompanying signals.

Two diacrylate crosslinkers containing cyclobutane-based mechanophores were chosen (crosslinker I and II, **Figure 1c**) to form a side-chain cross-linked first network. The difference in the substituents on the cyclobutane ring leads to substantial differences in the activation force of these two mechanophores. As suggested by the density functional theory calculation (**Figure S1,2**) and by single-molecule force spectroscopy,[16,24] the activation force necessary to achieve force-coupled unimolecular ring-opening reaction with a rate constant of approximately 10 s^{-1} at room temperature, f_a, is ~ 0.8 nN and ~ 2.5 nN for crosslinker I and crosslinker II, respectively. The force-induced scissile cycloreversion of the cyclobutane ring generates two C=C double bonds, resulting in the formation of two cinnamate groups in which the generated alkene is conjugated with the existing benzene ring and ester group (**Figure 1d**).[36,37] To investigate how other bonds in the first network influence the activation of cyclobutane mechanophore, a strong diacrylate crosslinker without cyclobutane ring (III, f_a ~ 3.4 nN) and a weak diacrylate azo crosslinker (IV, f_a ~ 1.6 nN) were also adopted.[20] In contrast to crosslinkers I and II, bond rupture in crosslinkers III and IV generates mechanoradicals. Moreover, the homolytic cleavage of C-C bonds in the main chain backbone (f_a > 3.0 nN) also generates mechanoradicals.[12,20,38] The differences in the products of various force-activated reactions allow the bond rupture sites to be characterized by different methods. The concentration of generated cinnamates from scission of cyclobutane mechanophores I and II can be quantified by taking advantage of the strong UV absorption of cinnamate groups,[37] while the mechanoradicals generated by scission of crosslinkers III and IV or of non-specific main chain bonds can be detected by Fenton color reaction.[12,39] In this way, we can distinguish the bond rupture sites in the first network and quantitatively evaluate how the activation force of mechanophores affects its activation selectivity and efficiency. The activation forces and products of various mechanophores and main chain backbone are summarized in Table 1. In the following discussion, we have utilized calculated f_a values. Due to the computational cost, we adopted the value of ~3.4 nN as the f_a of the PAMPS main chain, which was obtained from the calculation of a PAMPS analogues with -SO_3Na group simplified by -H (**Figure S1**). For ease of description, we define "weak" species with activation force less than half of strong common covalent bonds of 3.4 nN. "Medium" species are defined with activation force greater than half but at least 0.5 nN lower than typical covalent bonds.

Table 1. Activation force, f_a, and bond rupture products for various bonds in mechanophores and polymers. The rate constant for force-coupled bond activation used in the calculation is approximately 10 s^{-1}.

species		f_a, calculated	f_a, experimental[16,24]	products
linker	I, weak	0.8 nN	0.7 nN	C=C
	II, medium	2.5 nN	2.1 nN	C=C
	III, strong	3.4 nN	/	radical
	IV, weak	1.6 nN	/	radical
main chain	PAMPS, strong	> 3.0 nN (3.4 nN for PAMPS analogues)	/	radical

3. Experimental

3.1 Preparation and characterization of the double network hydrogels.

Seven types of DN gels were synthesized via a two-step sequential free radical polymerization process as illustrated in **Figure S3**. Three different single crosslinkers (I, II, and III) and four different mixed crosslinkers (I+III, I+IV, II+III, II+IV) of equal mole ratio of each crosslinker were used in the preparation of the first PAMPS network. The concentration of AMPS monomer was 1 M, and the concentration of initiator 2,2'-azobis(2,4-dimethyl) valeronitrile was 10 mM. The total crosslinker concentration in feed during the polymerization of the first network, C_1, was varied from 40 mM to 60 mM. For the second PAAm network, 2 M monomer AAm and 0.2 mM crosslinker *N*, *N*′-methylenebis(acrylamide) (MBA) were used for all DN gels (**Supporting Information**). The obtained DN gels are denoted according to the first network crosslinkers as DN-X-Y, where X represents the crosslinker species and Y represents the crosslinker concentration used in the preparation of the first network. For example, DN-I-60 represents DN gels with 60 mM crosslinker I used in the preparation of first PAMPS network. DN-I+III-60 represents DN gels with 30 mM I and 30 mM III crosslinker used in the preparation of first network. The mechanical properties of DN gels were characterized by the uniaxial tensile test.

During the preparation of DN gels, the Young's modulus of the as-prepared first PAMPS network $E_{1,0}$ was measured to evaluate the number density of elastically effective PAMPS strands in this as-prepared state ($\nu_{1,0}$). We adopted the phantom network model to estimate $\nu_{1,0}$ for a network with four-branched crosslinking points,[40] $\nu_{1,0} = 2E_{1,0}/3RT$, where R and T are the gas constant and absolute temperature, respectively. The ratio of the length of a single dimension in the equilibrated DN gels relative to that in the as-prepared PAMPS single network, λ_s, was also recorded to evaluate the elastically effective PAMPS strands density at the equilibrated state of DN gels, ν_1, where $\nu_1 = \nu_{1,0} / \lambda_s^3$.

Note that only a small fraction of crosslinkers in feed end up functioning as linking points. To assess the activation

efficiency of cyclobutane mechanophore in the polymer network, the concentration of elastically active mechanophores, C_{mp}, is needed. In a single-linker system, C_{mp} is equal to the concentration of total effective linking points, which is half of ν_1,[40] giving $C_{mp} = \nu_1 / 2$. In a 50:50 mixed-linker system crosslinker, we assume equal reactivity for each crosslinker during network formation and C_{mp} is considered half of the concentration of the total effective linking points, resulting in $C_{mp} = \nu_1 / 4$. Here, we treat the contribution of trapped entanglements to the modulus of the first network as being negligible, due to the high crosslinker stoichiometry relative to the AMPS monomer.

3.2 Measurement of C=C bonds concentration and mechanoradical concentration after stretching. The concentration of generated carbon-carbon double bonds ($C_{C=C}$) was estimated through the UV characteristic absorption of cinnamate esters at 290 nm (**Figure S4**). Unstretched pristine DN gels exhibited no absorbance at 290 nm. The absorbance at 290 nm appeared after stretching, indicating the formation of cinnamate ester. The concentration of cinnamate ester, equivalent to $C_{C=C}$, was determined by directly comparing the normalized absorbance (obtained by dividing the measured absorbance by the sample thickness to mitigate the effect of sample thickness) at 290 nm of stretched DN gels with calibration curves.

The mechanoradical concentration was estimated using the Fenton color reaction (**Figure S5,6**).[12,39] DN gels were immersed into an aqueous solution containing ferrous ion (Fe^{2+}) and xylenol orange (XO) to reach the equilibrium. Unstretched DN gels fed with Fe^{2+} and XO exhibited a yellow color with no absorbance at 580 nm. The color changed from yellow to brown, and absorbance at 580 nm appeared after stretching, indicating the formation of XO-Fe^{3+} complex, where ferric ion Fe^{3+} was derived from the oxidation-reduction reaction between Fe^{2+} and mechanoradicals. The concentration of Fe^{3+}, approximately equal to the C_{rad}, was determined by comparing the normalized absorbance at 580 nm with calibration curves.

For samples in which a necked region and unnecked region co-exist, both regions were measured. Detailed synthetic procedures and bond rupture product measurement are provided in the supporting information.

4. Results and discussion

4.1 Activation competition between the mechanophore and non-specific bond rupture

We first investigated the bond rupture of first network when a single crosslinker (I, II, and III) was used. As shown in **Figures 2a, b and Figure S7**, at the same C_1, $E_{1,0}$ of as-prepared PAMPS single network (SN) gels and λ_s of equilibrated DN gels with three different crosslinkers displayed only minor difference, indicating highly similar PAMPS network structures were formed by these three different crosslinkers.

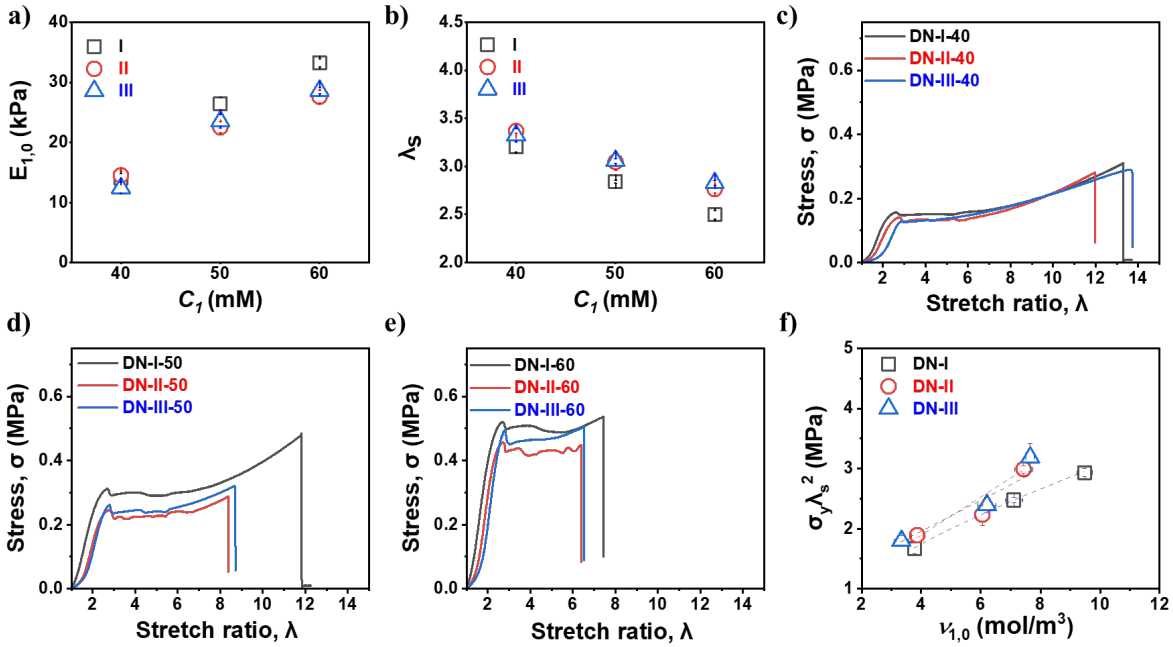

Figure 2. Mechanical properties of the gels crosslinked by a single type of crosslinker I, II, and III. (a) Young's modulus of the as-prepared PAMPS gels $E_{1,0}$ for different crosslinker concentration C_1. (b) Length swelling ratio (λ_s) of the PAMPS network in DN gels for different C_1. (c-e) Tensile stress-stretch ratio curves of the DN-I, DN-II, and DN-III gels for different C_1. (f) The rescaled yield stress $\sigma_y\lambda_s^2$ as a function of the number density of the elastic strands in the as-prepared PAMPS network ($\nu_{1,0}$). The error bars represent the standard deviations among at least three measurements.

Figures 2c-e show the stress-stretch ratio curves of the DN gels associated with each of the aforementioned first networks: DN-I-Y (Y = 40, 50, 60), DN-II-Y (Y = 40, 50, 60), and DN-III-Y (Y = 40, 50, 60). All DN's exhibited distinct

yielding and necking phenomenon.[34] That is, beyond the yielding point, the DN gels exhibit coexistence of a soft region and a hard region along the tensile direction. In the soft region, known as the necked region, substantial internal fracture of the first network has occurred and the second network carries the transferred load.[41,42] The necking zone then develops to span the whole sample with increased stretching. Remarkably, there is only a slight difference in the mechanical properties, including yield stress σ_y and yield stretch ratio λ_y, between the three DN gels (**Figure S8**). To remove the effect induced by variation in the number density of elastically effective strands in the equilibrated DN gels, we compared the rescaled yield stress ($\sigma_y\lambda_s^2$) at the same $\nu_{1,0}$ by taking as-prepared first network as a reference state, as reported previously.[33,43] **Figure 2f** illustrates that the rescaled yield stress for the three DN gels is nearly identical at the same $\nu_{1,0}$. These results indicate that the activation force of the crosslinker had a minimal effect on the yielding behavior of the gels in this work.

To examine the differences in the bond rupture site and density in the first network, pure DN gels or DN gels fed with Fe^{2+} and XO were stretched to a preset stretch ratio and then unloaded for the UV measurement (**Figure 3a**). Here, the preset stretch ratio was chosen at λ = 6, which is well beyond the yield point of these DNs but still not reaching the strain-hardening region. Before the yielding point, only a small proportion of the short strands within the first network experience rupture, so that the output bond rupture signal is too weak to be accurately measured. Only after reaching the yielding point, extensive bond rupture in the first network occurs in the necked region and gives an enhanced chemical signal. Such strain-dependent internal fracture in the first network was confirmed in this work (**Figure S9**). Prevention from reaching the strain-hardening region can avoid the bond rupture in the second network.[34]

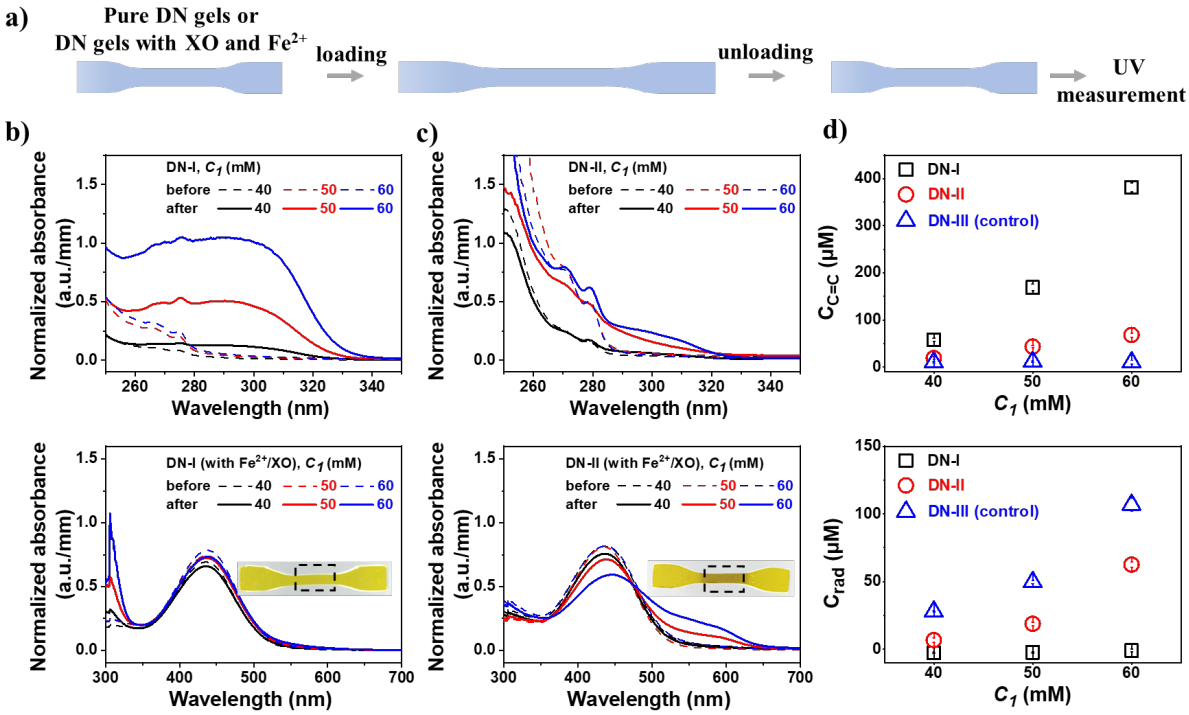

Figure 3. Bond rupture site in DN gels after stretching when crosslinked by different single crosslinkers. (a) Illustration of the stretching process to measure the bond rupture product in the first network. A pure DN gel or a DN gel with ferrous ion (Fe^{2+}) and xylenol orange (XO) was stretched to a preset stretch ratio of 6, then unloaded to the initial length. The necked region was cut for the UV measurement. (b) UV spectrums of pure DN-I gels (top) and DN-I gels fed with Fe^{2+} and XO (bottom) before and after stretching at different C_1. (c) UV spectrums of pure DN-II gels (top) and DN-II gels fed with Fe^{2+} and XO (bottom) before and after stretching at different C_1. The image inset in the bottom panel of b and c is the picture of DN gel fed with Fe^{2+} and XO after stretching. (d) The C=C bond concentration $C_{C=C}$ (top) and the mechanoradical concentration C_{rad} (bottom) generated in stretched DN gels at different C_1. The error bars represent the standard deviations among at least three measurements.

Figures 3b-d indicate the formation of the cinnamate product of crosslinker rupture in the necked DN-I and DN-II gels. Before stretching, pure DN-I gels with varied C_1 exhibited no UV absorbance at 290 nm **(Figure 3b)**. Upon stretching to necking, a distinct UV absorbance at 290 nm appeared, indicating the formation of C=C bonds and the force-induced cycloreversion of cyclobutane ring. The concentration of generated C=C bonds ($C_{C=C}$) in the necked region was evaluated to be 66 μM, 169 μM, and 381 μM for DN-I-40, DN-I-50, and DN-I-60, respectively (**Figure 3d**). The increase of $C_{C=C}$ with C_1 is attributed to the increase of the PAMPS network density at the swelling equilibrated

state (ν_1) at which the mechanical deformation was performed. However, DN-I gels fed with Fe^{2+} and XO did not show any UV absorbance at 580 nm after stretching and, consequently, no color change in the necked region. The lack of Fenton chemistry suggests that no mechanoradicals were generated in DN-I gels. In contrast, DN-III generated a large number of mechanoradicals upon stretching (**Figure S10**). Thus, in DN-I gels, the mechanophores were selectively activated by the applied mechanical stress, with almost no non-specific homolytic bond scission.

In comparison, at the same C_1, the UV absorbance at 290 nm in stretched DN-II gels was considerably lower than DN-I gels (**Figure 3c, d**). The concentration of generated C=C bonds was found to be 19 μM, 43 μM, and 68 μM for DN-II-40, DN-II-50, and DN-II-60, respectively. The most significant difference between DN-II and DN-I gels is that DN-II gels fed with Fe^{2+} and XO showed strong absorbance at 580 nm and exhibited color change from yellow to brown after stretching, similar to the DN-III gels. This result indicates the formation of mechanoradicals in stretched DN-II gels. The generated mechanoradical concentration was evaluated to be 11 μM, 22 μM, and 66 μM for DN-II-40, DN-II-50, and DN-II-60, respectively. These collective findings clearly demonstrate that, in DN-II gels, in addition to the activation of the cyclobutane mechanophore, a comparable amount of non-specific bond rupture simultaneously occurred in the main chain backbone under external force.

To further discuss the effect of activation force of mechanophores on the activation efficiency and selectivity, we estimated two quantities. One is the activation efficiency (AE), defined as the percentage of activated cyclobutane mechanophores among the mechanophores effectively incorporated as linking points in the gel synthesis. It can be calculated using $AE = (C_{C=C} / 2) / C_{mp} \times 100\%$.

The other is the activation selectivity of cyclobutane mechanophore AS, defined as the percentage of bond rupture in the cyclobutane mechanophore among the total bond rupture in the first network. It can be calculated using $AS = C_{C=C} / (C_{C=C} + C_{rad}) \times 100\%$.

Crosslinker I has an extremely low activation force relative to the polymer main chain ($f_{a\text{-I}} / f_{a\text{-chain}}$ = 0.8 nN / 3.4 nN), and we find that AE = 60% and AS = 100% in DN-I gels (**Figure 4a, b**). In contrast, crosslinker II has an intermediate activation force ($f_{a\text{-II}} / f_{a\text{-chain}}$ = 2.5 nN / 3.4 nN), and for DN-II gels, AE = 10% while AS = 60%. Thus, the difference in f_a has a substantial impact on both the selectivity and overall efficiency of crosslinker scission.

Either the generated C=C bonds or the mechanoradicals were derived from the bond rupture in the first network after stretching. Thus, we can evaluate the percentage of the total ruptured bonds among the elastically effective PAMPS strands, φ_T, using the formula $\varphi_T = (C_{C=C} + C_{rad}) / 2 / \nu_1 \times 100\%$. As depicted in **Figure 4c**, due to the contribution of non-specific bond rupture, the φ_T values of DN-II gels remained lower compared to those of DN-I gels, but approached the levels observed in DN-III gels.

The irreversible bond rupture of the first network led to the large hysteresis in the DN gels during loading-unloading cyclic tensile tests (**Figure S11**).[44] Interestingly, despite noticeable variations in the bond rupture sites and quantity among the three gels, the hysteresis energy density at the same C_1 and at the same yield stress was remarkably consistent. It indicates that the specific details of the bond rupture propagation process in the first network had a limited effect on the hysteresis of the DN gels. Besides, the observation of the same dissipated energy but more bond rupture in DN-I gels indicates that the dissipated energy per bond scission is significantly lower for weak crosslinker I, which can be attributed to its lower activation force.

With the detailed information on the bond rupture site in the first network provided above, we can elucidate the role of the mechanophore's activation force on its scissile activation when embedded in an inhomogeneous network as a crosslinker. The first network formed by free radical polymerization shows high structural inhomogeneity.[45] Due to the wide distribution of strand length and resulting different angles of force exertion (**Figure 4e,f**), the ratio of force exerted on the crosslinker to the maximum force exerted on the neighboring main chain $K = f_{linker} / f_{chain}$ shows a wide distribution. This broad distribution of K can explain why, at the same activation force of the main chain $f_{a\text{-chain}}$, altering the activation force of the mechanophores in crosslinker $f_{a\text{-linker}}$ can impact the activation selectivity of the mechanophore. When extensive bond rupture of first network occurs, the bond rupture point will lie in the crosslinker for those $K > f_{a\text{-linker}} / f_{a\text{-chain}}$ and the bond rupture point will lie in other non-specific point in the main chain for those $K < f_{a\text{-linker}} / f_{a\text{-chain}}$. Thus, even though $f_{a\text{-linker}}$ of II is smaller than $f_{a\text{-chain}}$ ($f_{a\text{-II}} / f_{a\text{-chain}}$ = 0.73), only a 60% activation selectivity was achieved. The 40% non-specific bond ruptures suggest the involvement of approximately 40% of linking points where K < 0.73. With the $f_{a\text{-linker}}$ of I deceased to 0.8 nN ($f_{a\text{-I}} / f_{a\text{-chain}}$ = 0.23), almost no non-specific bond rupture occurred, indicating there are few linking points where force on the crosslinker is less than 0.23 times the force on connected main chain.

It should be noted that rupture at different sites results in different stress release and redistribution on the surviving network. Rupture of the crosslinker I and II only partially unloads the force on the polymer strands and lengthens the strands.[16] During the force redistribution after bond rupture, the lengthened strands are advantageous for transferring the load to remote regions and inducing the bond scissions in these areas. In contrast, rupture of the main chain backbone fully unloads the strands. Consequently, a weak crosslinker I, with 100% bond rupture located at the crosslinking points, can induce a higher total bond scission in the network when compared to a medium crosslinker II and a strong crosslinker III.

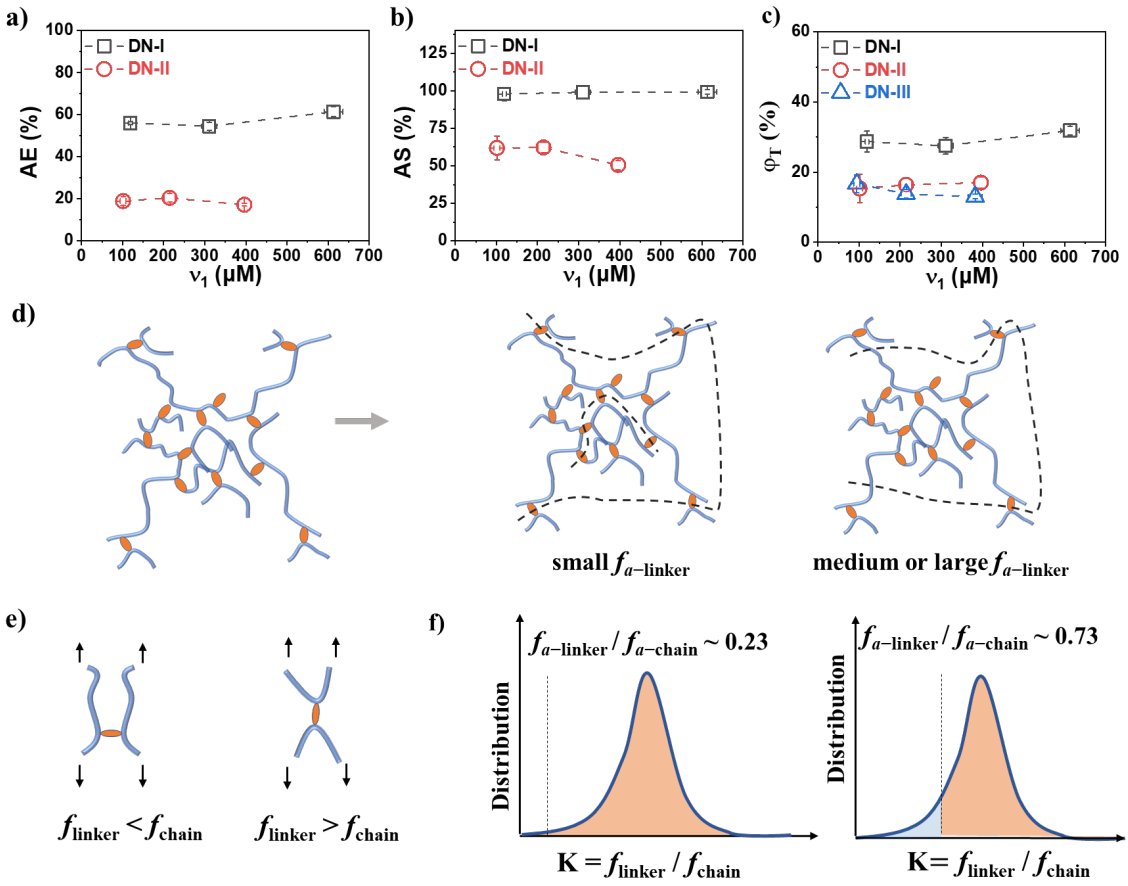

Figure 4. The effect of activation force on the competition between selective mechanophore activation and non-specific bond scission. (a-c) The activation efficiency AE (the percentage of activated mechanophores among the total mechanophores effectively working as the linking points in the polymer network) (a), the activation selectivity AS (the percentage of bonds ruptured in mechanophores among the total ruptured bonds in the first network) (b), and the percentage of total broken bonds among the total elastically effective strands φ_T (c) in DN-I, DN-II, and DN-III gels after stretching. (d) Illustration of the effect of activation force of crosslinker $f_{a\text{-linker}}$ on the sites and numbers of the bond rupture for a heterogeneous network under the external force. Dashed lines represent the potential micro-crack propagation pathways. (e) Illustration of local chain structures for the cases that the force exerted on the crosslinker f_{linker} is smaller (left) or larger (right) than that on the mainchain backbone f_{chain}. (f) A schematic illustration of the force ratio f_{linker} / f_{chain} distribution on the crosslinker and on the mainchain backbone in a heterogeneous polymer network and its effect on the bond rupture sites. For linking points whose f_{linker} / f_{chain} is larger than $f_{a\text{-linker}}$ / $f_{a\text{-chain}}$ (orange region), the bond rupture sites are located in the crosslinker. And for linking points whose f_{linker} / f_{chain} is smaller than $f_{a\text{-linker}}$ / $f_{a\text{-chain}}$ (blue region), the bond rupture sites are located in the main chain. The left and right illustrations correspond to the case of DN-I ($f_{a\text{-linker}}$ / $f_{a\text{-chain}}$=0.23) and DN-II ($f_{a\text{-linker}}$ / $f_{a\text{-chain}}$= 0.73), respectively. The error bars represent the standard deviations among at least three measurements.

4.2 Activation competition between mixed mechanophores in crosslinkers

We then investigated the bond rupture of the first network when mixed crosslinkers were used. Four crosslinker mixtures, each comprising an equal mole ratio of individual crosslinkers, were selected based on the activation force: weak and strong (I+III), weak and weak (I+IV), medium and strong (II+III), medium and weak (II+IV). The values of $E_{1,0}$ and λ_s for these PAMPS SN gels were summarized in **Figure S12a,b**. In the $\lambda_s \sim \nu_{1,0}$ plot, all datasets are roughly aligned on the same line, indicating again the intrinsic correlation between these two parameters (**Figure S12c**). All DN gels with mixed mechanophores showed yielding behavior, and the yielding stress increased with the in-feed crosslinker concentration (**Figure S12d-g**). When comparing the rescaled yield stress $\sigma_y\lambda_s^2$ at the same $\nu_{1,0}$ to mitigate the effects of $E_{1,0}$ and λ_s, the scaling relationship $\sigma_y\lambda_s^2 \sim \nu_{1,0}$ for all these DN gels fell on the same curve, independent of the type of the mixed crosslinkers used (**Figure S12h**). Furthermore, the true yielding stress normalized to the as-prepared state of the PAMPS gel, $\sigma_y\lambda_y\lambda_s^3$, exhibited a constant value, independent of $\nu_{1,0}$ and the crosslinkers (**Figure S12i**).[43] These results are consistent with those obtained with a single crosslinker, suggesting that all DN gels had a similar network. Therefore, a comparison of mixed crosslinker to single crosslinker DN gels allows to elucidate the influence of one crosslinker in the presence of another.

The UV spectrum and corresponding concentrations of generated C=C bonds and mechanoradicals at varied in feed crosslinker concentration C_1 in above four sets of DN gels are shown in **Figure S13 and S14**. The slight difference of

$E_{1,0}$ and λ_s reflects a difference in the PAMPS strand density at the equilibrated state (ν_1), which in turn impacts the final concentration of bond rupture products. To mitigate the effects of differences in concentration, we compare the bond rupture products in DN gels at the same level of ν_1 in the following discussion.

Firstly, we investigated how the incorporation of strong crosslinker III influences the activation of weak crosslinker I by comparing DN-I+III gels (weak and strong, $f_{a\text{-I}}/f_{a\text{-III}}$ = 0.8 nN / 3.4 nN) with DN-I gels. As shown in **Figure 5a**, at the same ν_1, the $C_{C=C}$ in stretched DN-I+III gels were almost the same with that in DN-I gels. Thus, the average AE of crosslinker I in DN-I+III was almost two times higher than that in DN-I gels, since the amount of crosslinker I in DN-I+III was half of that in DN-I (**Figure 6a**). However, the mechanoradicals were still not detected in DN-I+III gels, indicating that the bond rupture points in the first network all still lay within the cyclobutane mechanophore (**Figure 5b and 6b**), achieving a 100% activation selectivity. These results indicate that network rupture can propagate selectively along the weak mechanophores as low activation force results in fast activation kinetics **(Figure 6g)**. The activation of weak crosslinker became more efficient in the presence of the strong crosslinker, while the activation of strong crosslinker was totally suppressed by the presence of weak crosslinker.

However, for DN-I+IV gels with two weak crosslinkers ($f_{a\text{-I}}/f_{a\text{-IV}}$ = 0.8 nN / 1.6 nN), the concentrations of generated C=C bonds after stretching decreased compared to DN-I gels. Besides, a large number of mechanoradicals was detected. Given that DN-I gels exhibited no non-specific bond rupture and did not generate mechanoradicals, the observed mechanoradicals are attributed to the activation of the azo-linker IV. AS of crosslinker I in DN-I+IV gels decreased to 45%-65% from a value of 100% in DN-I. The similar low activation forces of crosslinker I and crosslinker IV make them show a similar possibility of being activated during the bond rupture propagation. The total bonds broken in DN-I+IV gels after necking are at the same level observed in DN-I and DN-I+III gels (**Figure 6c**).

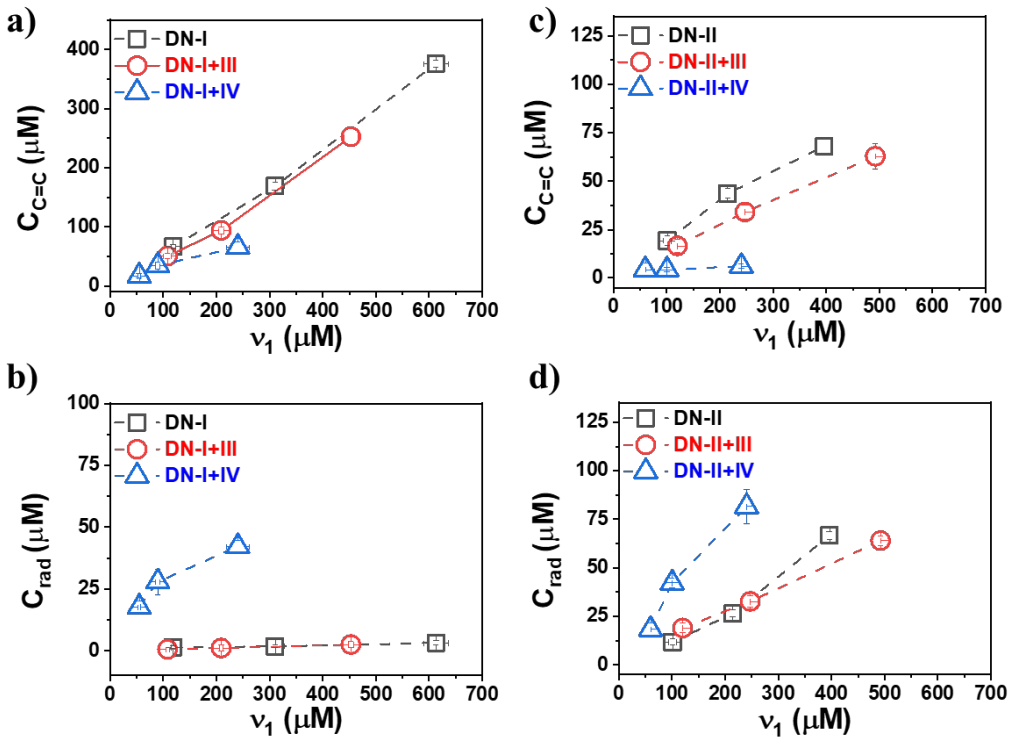

Figure 5. Bond rupture product in DN gels after stretching for the PAMPS network crosslinked by two mixed crosslinkers. (a,b) The generated C=C bond concentration $C_{C=C}$ (a) and the mechanoradical concentration C_{rad} (b) in DN-I+III and DN-I+IV gels as a function of the elastically effective PAMPS strands density at the equilibrated state ν_1. (c,d) $C_{C=C}$ (c) and C_{rad} (d) in DN-II+III and DN-II+IV gels as a function of ν_1. For comparison, $C_{C=C}$ and C_{rad} in DN-I and DN-II gels are also included. The error bars represent the standard deviations among at least three measurements.

Then we compare the activation differences in DN-II+III (medium and strong, $f_{a\text{-II}}/f_{a\text{-III}}$ = 2.5 nN / 3.4 nN) and DN-II+IV gels (medium and weak, $f_{a\text{-II}}/f_{a\text{-IV}}$ = 2.5 nN / 1.6 nN) after stretching in comparison to DN-II gels. As shown in **Figure 5c,d,** at the same ν_1, the concentration of generated C=C bonds in DN-II+III gels slightly decreased compared with DN-II gels, while the mechanoradical concentration didn't show an obvious increase. Consequently, AS of crosslinker II decreased from 60% to 50% and the percentage of total broken bonds φ_T decreased from 17% to 14% (**Figure 6d-f**), while AE of crosslinker II slightly increased from 20% to 27% due to the less amount of crosslinker II used. These results indicate that the addition of the strong crosslinker III mainly affected the concentration of the medium link II in the polymer network. However, in DN-II+IV gels, the C=C bonds were not detected after stretching. It indicates that the weak azo crosslinker IV totally suppressed the activation of the medium crosslinker

II, similar to the DN-I+III system. Meanwhile, the mechanoradical concentrations in DN-II+IV gels significantly increased, likely attributed to the efficient activation of weak azo-linker IV, resulting in a higher φ_T compare with DN-II and DN-II+III gels without weak crosslinkers.

Based on the obtained data, it is suggested that to achieve multiple mechanoresponsive functions with dual distinct mechanophores in a polymer network, both mechanophores should be mechanically weak, which in our system means that each has an activation force less than half of the other strong bonds. Although their activation forces may differ a few tenths of a nanonewton, simultaneous activation can occur. This phenomenon arises due to the heterogeneous distribution of tension in a polymer network, enabling the activation of stronger mechanophore in the tension concentrated region. This stands in contrast to a single polymer chain where tension remains uniform throughout and differences of a few 100 pN can lead to high selectivity for the lower force mechanophore. However, if a significant disparity in activation force exists between the mechanophores, where one is weak and the other is either medium or strong, in a polymer network, the distribution of tension in the polymer network proves insufficient to mitigate this disparity. The weaker mechanophore will be selectively activated in the network when subjected to mechanical forces while the stronger one is likely to be deactivated. Moreover, the combination of two medium/strong mechanophores leads to the simultaneous activation of the two mechanophores. However, this combination faces the limitation of low activation efficiency for both mechanophores and interferes with non-specific bond breakage.

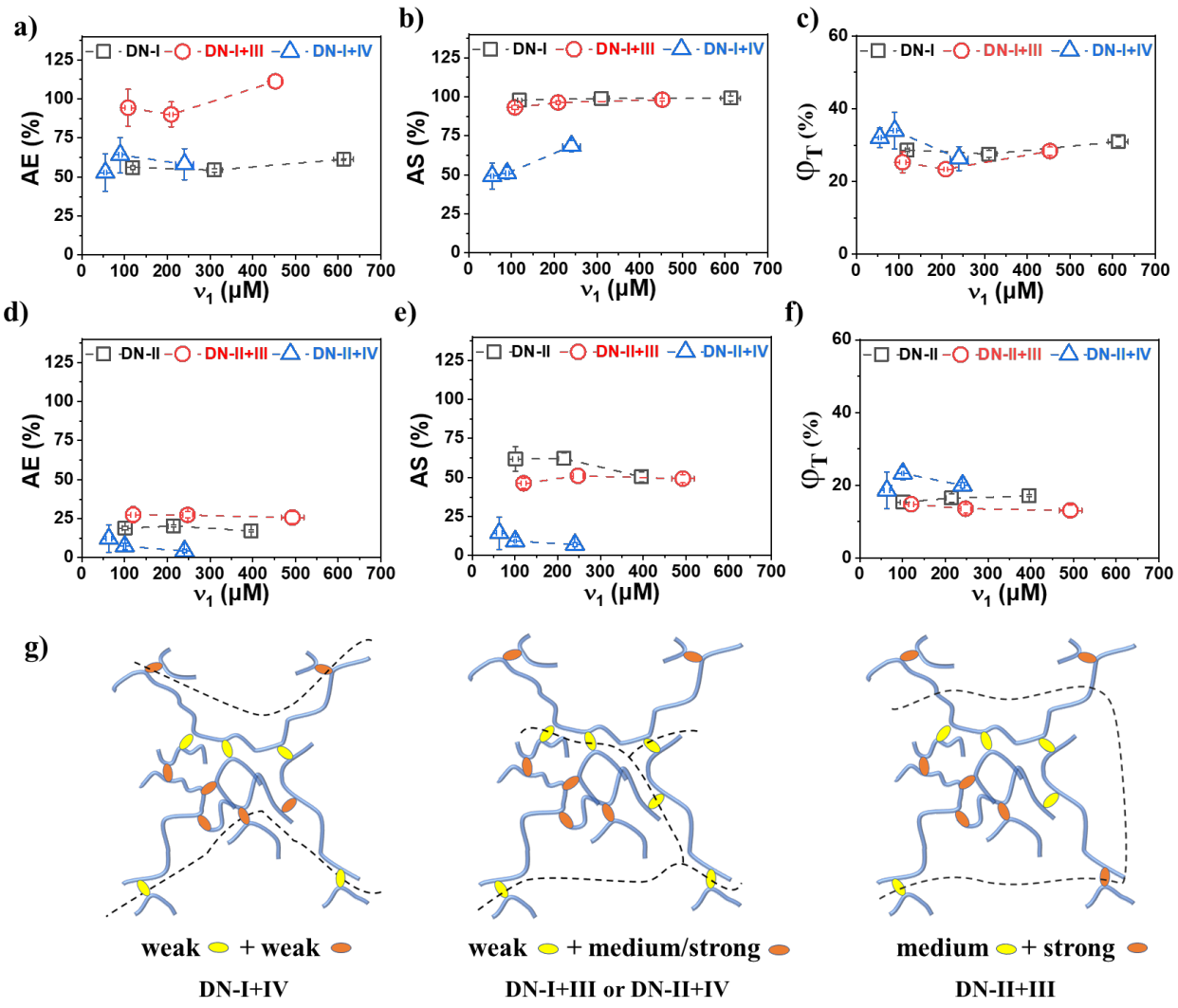

Figure 6. Activation competition between different mechanophores in crosslinkers. (a-c) The activation efficiency AE (a), the activation selectivity AS (b) of the cyclobutane mechanophore, and the percentage of total broken bonds out of the total elastically effective strands φ_T (c) in DN-I, DN-I+III, and DN-I+IV gels. (d-f) AE, AS, and φ_T in DN-II, DN-II+III, and DN-II+IV gels. (g) Illustration of the effect of different combinations of activation force on the sites and numbers of the bond rupture. The error bars represent the standard deviations among at least three measurements.

5. Conclusion

By quantitatively detecting the concentrations of C=C bonds and mechanoradicals after stretching, we have gained insights into the role of activation forces in the activation competition among mechanophores within a polymer network. When a single mechanophore is incorporated as the crosslinker, mechanophore activation faces the challenge of competing with non-specific bond ruptures. We observed that mechanophores with low activation force relative to other bonds in the polymer strand backbone ($f_{a\text{-I}}$ / $f_{a\text{-chain}}$ = 0.8 nN / 3.4 nN) could be activated with 100% selectivity. An increase in the activation force of the mechanophore ($f_{a\text{-II}}$ / $f_{a\text{-chain}}$ = 2.5 nN / 3.4 nN) led to a significant decrease in activation selectivity to ~ 60%, due to concomitant scission of a large number of non-specific bonds in the backbone. These findings not only provide crucial design principles for achieving selective mechanophore activation but also deepen our understanding of the damage mechanism within polymer networks when utilizing mechanophores as detectors.

Furthermore, when two mechanophore are incorporated in one polymer network as crosslinkers, mechanophore activation faces the competition from the other mechanophore, as well as non-specific bond cleavage in the backbone. We discovered that weak mechanophores can completely suppress the activation of medium or strong mechanophores (e.g., $f_{a\text{-I}}$ / $f_{a\text{-III}}$ = 0.8 nN / 3.4 nN). Therefore, when aiming to achieve multiple mechanoresponsive functions using two distinct mechanophores, it is important that both mechanophores exhibit proximate low activation forces. This research empowers us to exercise more precise control over mechanophore activation by fine-tuning the activation forces. Additionally, this work is poised to facilitate the application of multiple mechanophores in polymer materials for achieving programmed, diverse mechanoresponsive functions.

ASSOCIATED CONTENT

Supporting information. Details of the computational simulation, reagents used, synthesis procedure of crosslinkers and hydrogels, measurement of mechanoradical concentration and double bond concentration. This material is available free of charge via the Internet at http://pubs.acs.org.

AUTHOR INFORMATION

Corresponding Author

* stephen.craig@duke.edu; gong@sci.hokudai.ac.jp

Author contributions

#Z. J. Wang and S. Wang contributed equally. Z.J.W., S.L.C. and J.P.G. conceived the study. Z.J.W and S.W. performed the experiments. J.J. and S.M. performed simulations. Y.H. helped perform the experiments. T.N., S.L.C. and J.P.G. supervised the study. All authors discussed the results and Z.J.W. wrote the manuscript with the input of all the authors.

ACKNOWLEDGMENT

T.N. and J.P.G. acknowledge the funding support from JSPS KAKENHI, grant number JP22H04968, JP22K21342, and JST, PRESTO, grant number JPMJPR2098, Japan. This work of S.W. and S.L.C. was supported by the NSF Center for the Chemistry of Molecularly Optimized Networks (MONET) (CHE-2116298 to S.L.C.).

REFERENCES

(1) Ghanem, M. A.; Basu, A.; Behrou, R.; Boechler, N.; Boydston, A. J.; Craig, S. L.; Lin, Y.; Lynde, B. E.; Nelson, A.; Shen, H.; Storti, D. W. The Role of Polymer Mechanochemistry in Responsive Materials and Additive Manufacturing. *Nat. Rev. Mater.* **2020**, *6*, 84-98.

(2) Li, J.; Nagamani, C.; Moore, J. S. Polymer Mechanochemistry: from Destructive to Productive. *Acc. Chem. Res.* **2015**, *48*, 2181-2190.

(3) Piermattei, A.; Karthikeyan, S.; Sijbesma, R. P. Activating Catalysts with Mechanical Force. *Nat. Chem.* **2009**, *1*, 133-137.

(4) Davis, D. A.; Hamilton, A.; Yang, J.; Cremar, L. D.; Van Gough, D.; Potisek, S. L.; Ong, M. T.; Braun, P. V.; Martinez, T. J.; White, S. R.; Moore, J. S.; Sottos, N. R. Force-Induced Activation of Covalent Bonds in Mechanoresponsive Polymeric Materials. *Nature* **2009**, *459*, 68-72.

(5) Ducrot, E.; Chen, Y.; Bulters, M.; Sijbesma, R. P.; Creton, C. Toughening Elastomers with Sacrificial Bonds and Watching Them Break. *Science* **2014**, *344*, 186-189.

(6) Kosuge, T.; Zhu, X.; Lau, V. M.; Aoki, D.; Martinez, T. J.; Moore, J. S.; Otsuka, H. Multicolor Mechanochromism of a Polymer/Silica Composite with Dual Distinct Mechanophores. *J. Am. Chem. Soc.* **2019**, *141*, 1898-1902.

(7) Gunckel, R.; Koo, B.; Xu, Y.; Pauley, B.; Hall, A.; Chattopadhyay, A.; Dai, L. L. Grafted Cinnamoyl-Based Mechanophores for Self-Sensing and Photochemical Healing Capabilities in Epoxy. *ACS Appl. Polym. Mater.* **2020**, *2*, 3916-3928.

(8) Chen, Y.; Yeh, C. J.; Qi, Y.; Long, R.; Creton, C. From Force-Responsive Molecules to Quantifying and Mapping Stresses in Soft Materials. *Sci. Adv.* **2020**, *6*, eaaz5093.

(9) Baumann, C.; Stratigaki, M.; Centeno, S. P.; Gostl, R. Multicolor Mechanofluorophores for the Quantitative Detection of Covalent Bond Scission in Polymers. *Angew. Chem. Int. Ed.* **2021**, *60*, 13287-13293.

(10) Yamakado, T.; Saito, S. Ratiometric Flapping Force Probe That Works in Polymer Gels. *J. Am. Chem. Soc.* **2022**, *144*, 2804-2815.

(11) Ramirez, A. L.; Kean, Z. S.; Orlicki, J. A.; Champhekar, M.; Elsakr, S. M.; Krause, W. E.; Craig, S. L. Mechanochemical Strengthening of a Synthetic Polymer in Response to Typically Destructive Shear Forces. *Nat. Chem.* **2013**, *5*, 757-761.

(12) Matsuda, T.; Kawakami, R.; Namba, R.; Nakajima, T.; Gong, J. P. Mechanoresponsive Self-Growing Hydrogels Inspired by Muscle Training. *Science* **2019**, *363*, 504-508.

(13) Wang, Z.; Zheng, X.; Ouchi, T.; Kouznetsova, T. B.; Beech, H. K.; Av-Ron, S.; Matsuda, T.; Bowser, B. H.; Wang, S.; Johnson, J. A.; Kalow, J. A.; Olsen, B. D.; Gong, J. P.; Rubinstein, M.; Craig, S. L. Toughening Hydrogels Through Force-Triggered Chemical Reactions That Lengthen Polymer Strands. *Science* **2021**, *374*, 193-196.

(14) Du, M.; Houck, H. A.; Yin, Q.; Xu, Y.; Huang, Y.; Lan, Y.; Yang, L.; Du Prez, F. E.; Chang, G. Force-Reversible Chemical Reaction at Ambient Temperature for Designing Toughened Dynamic Covalent Polymer Networks. *Nat. Commun.* **2022**, *13*, 3231.

(15) Watabe, T.; Aoki, D.; Otsuka, H. Polymer-Network Toughening and Highly Sensitive Mechanochromism via a Dynamic Covalent Mechanophore and a Multinetwork Strategy. *Macromolecules* **2022**, *55*, 5795-5802.

(16) Wang, S.; Hu, Y.; Kouznetsova, T. B.; Sapir, L.; Chen, D.; Herzog-Arbeitman, D.; Johnson, A. J.; Rubinstein, M.; Craig, S. L. Facile Mechanochemical Cycloreversion of Polymer Cross-Linkers Enhances Tear Resistance. *Science* **2023**, *380*, 1248–1252.

(17) Kung, R.; Gostl, R.; Schmidt, B. M. Release of Molecular Cargo from Polymer Systems by Mechanochemistry. *Chemistry* **2022**, *28*, e202103860.

(18) Ouchi, T.; Bowser, B. H.; Kouznetsova, T. B.; Zheng, X.; Craig, S. L. Strain-Triggered Acidification in A Double-Network Hydrogel Enabled by Multi-Functional Transduction of Molecular Mechanochemistry. *Mater. Horiz.* **2023**, *10*, 585-593.

(19) Hu, X.; Zeng, T.; Husic, C. C.; Robb, M. J. Mechanically Triggered Small Molecule Release from a Masked Furfuryl Carbonate. *J. Am. Chem. Soc.* **2019**, *141*, 15018-15023.

(20) Wang, Z. J.; Jiang, J.; Mu, Q.; Maeda, S.; Nakajima, T.; Gong, J. P. Azo-Crosslinked Double-Network Hydrogels Enabling Highly Efficient Mechanoradical Generation. *J. Am. Chem. Soc.* **2022**, *144*, 3154-3161.

(21) Berkowski, K. L.; Potisek, S. L.; Hickenboth, C. R.; Moore, J. S. Ultrasound-Induced Site-Specific Cleavage of Azo-Functionalized Poly(ethylene glycol). *Macromolecules* **2005**, *38*, 8975-8978.

(22) Lin, Y.; Barbee, M. H.; Chang, C. C.; Craig, S. L. Regiochemical Effects on Mechanophore Activation in Bulk Materials. *J. Am. Chem. Soc.* **2018**, *140*, 15969-15975.

(23) Wang, S.; Beech, H. K.; Bowser, B. H.; Kouznetsova, T. B.; Olsen, B. D.; Rubinstein, M.; Craig, S. L. Mechanism Dictates Mechanics: A Molecular Substituent Effect in the Macroscopic Fracture of a Covalent Polymer Network. *J. Am. Chem. Soc.* **2021**, *143*, 3714-3718.

(24) Bowser, B. H.; Wang, S.; Kouznetsova, T. B.; Beech, H. K.; Olsen, B. D.; Rubinstein, M.; Craig, S. L. Single-Event Spectroscopy and Unravelling Kinetics of Covalent Domains Based on Cyclobutane Mechanophores. *J. Am. Chem. Soc.* **2021**, *143*, 5269-5276.

(25) Kryger, M. J.; Munaretto, A. M.; Moore, J. S. Structure–Mechanochemical Activity Relationships for Cyclobutane Mechanophores. *J. Am. Chem. Soc.* **2011**, *133*, 18992–18998.

(26) Kumar, S.; Stauch, T. The Activation Efficiency of Mechanophores Can Be Modulated by Adjacent Polymer Composition. *RSC Adv.* **2021**, *11*, 7391-7396.

(27) Overholts, A. C.; Robb, M. J. Examining the Impact of Relative Mechanophore Activity on the Selectivity of Ultrasound-Induced Mechanochemical Chain Scission. *ACS Macro Lett.* **2022**, *11*, 733-738.

(28) Kim, T. A.; Lamuta, C.; Kim, H.; Leal, C.; Sottos, N. R. Interfacial Force-Focusing Effect in Mechanophore-Linked Nanocomposites. *Adv. Sci.* **2020**, *7*, 1903464.

(29) Park, J.; Lee, Y.; Barbee, M. H.; Cho, S.; Cho, S.; Shanker, R.; Kim, J.; Myoung, J.; Kim, M. P.; Baig, C.; Craig, S. L.; Ko, H. A Hierarchical Nanoparticle-in-Micropore Architecture for Enhanced Mechanosensitivity and Stretchability in Mechanochromic Electronic Skins. *Adv. Mater.* **2019**, *31*, e1808148.

(30) Dubach, F. F. C.; Ellenbroek, W. G.; Storm, C. How Accurately Do Mechanophores Report on Bond Scission in Soft Polymer Materials? *J. Polym Sci.* **2021**, *59*, 1188-1199.

(31) Kean, Z. S.; Gossweiler, G. R.; Kouznetsova, T. B.; Hewage, G. B.; Craig, S. L. A Coumarin Dimer Probe of Mechanochemical Scission Efficiency in the Sonochemical Activation of Chain-centered Mechanophore Polymers. *Chem. Commun.* **2015**, *51*, 9157-9160.

(32) Lloyd, E. M.; Vakil, J. R.; Yao, Y., Sottos, N. R.; Craig, S. L. Covalent Mechanochemistry and Contemporary Polymer Network Chemistry: A Marriage in the Making. *J. Am. Chem. Soc.* **2023**, *145*, 751–768.

(33) Gong, J. P.; Katsuyama, Y.; Kurokawa, T.; Osada, Y. Double-Network Hydrogels with Extremely High Mechanical Strength. *Adv. Mater.* **2003**, *15*, 1155-1158.

(34) Na H.; Tanaka, Y.; Kawauchi, Y.; Furukawa, H.; Sumiyoshi, T.; Gong, J. P.; Osada, Y. Necking Phenomenon of Double-Network Gels. *Macromolecules* **2006**, *39*, 4641-4645.

(35) Nakajima, T.; Kurokawa, T.; Furukawa, H.; Gong, J. P. Effect of the Constituent Networks of Double-Network Gels on Their Mechanical Properties and Energy Dissipation Process. *Soft Matter* **2020**, *16*, 8618-8627.

(36) Feng, L.; Romulus, J.; Li, M.; Sha, R.; Royer, J.; Wu, K. T.; Xu, Q.; Seeman, N. C.; Weck, M.; Chaikin, P. Cinnamate-Based DNA Photolithography. *Nat. Mater.* **2013**, *12*, 747-753.

(37) Li, X.; Cui, J.; Zhang, W.; Huang, J.; Li, W.; Lin, C.; Jiang, Y.; Zhang, Y.; Li, G. Controllable Photo-Switching of Cinnamate-Based Photonic Films with Remarkable Stability. *J. Mater. Chem.* **2011**, *21*, 17953–17959.

(38) Zheng. Y.; Jiang, J.; Jin, M.; Miura, D.; Lu, F. X.; Kubota, K.; Nakajima, T.; Maeda, S.; Ito, H.; Gong, J. P. In Situ and Real-Time Visualization of Mechanochemical Damage in Double-Network Hydrogels by Prefluorescent Probe via Oxygen Relayed Radical Trappin. *J. Am. Chem. Soc.* **2023**, *145*, 7376-7389.

(39) Gay, G.; Collins, J.; Gebicki, J. M. Determination of Iron in Solutions with the Ferric–Xylenol Orange Complex. *Anal. Biochem.* **1999**, *273*, 143–148.

(40) Rubinstein, M.; Colby, R. *Polymer Physics* **2003**, pp 262–266.

(41) Fukao, K.; Nakajima, T.; Nonoyama, T.; Kurokawa, T.; Kawai, T.; Gong, J. P. Effect of Relative Strength of Two Networks on the Internal Fracture Process of Double Network Hydrogels as Revealed by in Situ Small-Angle X-ray Scattering. *Macromolecules* **2020**, *53*, 1154-1163.

(42) Chen, Y.; Sanoja, G.; Creton, C. Mechanochemistry Unveils Stress Transfer During Sacrificial Bond Fracture of Tough Multiple Network Elastomers. *Chem. Sci.* **2021**, *12*, 11098-11108.

(43) Zheng, Y.; Nakajima, T.; Cui, W.; Hui, C.; Gong, J. P. Swelling Effect on the Yielding, Elasticity, and Fracture of Double Network Hydrogels with an Inhomogeneous First Network. *Macromolecules* **2023**, *56*, 3962–3972.

(44) Webber, R. E.; Creton, C.; Brown, H.; Gong, J. P. Large Strain Hysteresis and Mullins Effect of Tough Double-Network Hydrogels. *Macromolecules* **2007**, *40*, 2919–2927.

(45) Kiyama, R.; Yoshida, M.; Nonoyama, T.; Sedlacik, T.; Jinnai, H.; Kurokawa, T.; Nakajima, T.; Gong, J. P. Nanoscale TEM Imaging of Hydrogel Network Architecture. *Adv. Mater.* **2022**, e2208902.

SYNOPSIS TOC